Research Article | Vol. 25, No. 19 | 18 Sep 2017 | OPTICS EXPRESS 22905
Optics EXPRESS

Wideband backscattering reduction at terahertz using compound reflection grating

BAKHTIYAR ORAZBAYEV,[1] PABLO RODRÍGUEZ-ULIBARRI,[1] AND MIGUEL BERUETE[1,2,*]

[1]*Antennas Group-TERALAB, Universidad Pública de Navarra, 31006 Pamplona, Spain*
[2]*Institute of Smart Cities, Public University of Navarra, 31006 Pamplona, Spain*
**miguel.beruete@unavarra.es*

Abstract: Backscattering reduction is usually achieved by using either absorbers or diffractions gratings at the expense of a narrow bandwidth. In this paper, we propose a different strategy based on a metallic compound reflection grating (CRG). We demonstrate that this structure allows a strong and broadband (fractional bandwidth, FBW ≈57%) backscattering reduction in the terahertz (THz) range by efficiently transferring the incident energy to the diffracted modes. The design is analyzed in terms of equivalent circuit and numerical simulations and the results are corroborated by a manufactured prototype operating at 0.35 THz.

© 2017 Optical Society of America

OCIS codes: (050.1950) Diffraction gratings; (290.1350) Backscattering.

References and links

1. H. Singh and R. M. Jha, *Active Radar Cross Section Reduction* (Cambridge University Press, 2015).
2. L.-H. Du, J. Li, Z.-H. Zhai, K. Meng, Q. Liu, S.-C. Zhong, P.-W. Zhou, L.-G. Zhu, Z.-R. Li, and Q.-X. Peng, "A high-performance broadband terahertz absorber based on sawtooth-shape doped-silicon," AIP Adv. **6**(5), 55112 (2016).
3. H. Xiong, J.-S. Hong, C.-M. Luo, and L.-L. Zhong, "An ultrathin and broadband metamaterial absorber using multi-layer structures," J. Appl. Phys. **114**(6), 64109 (2013).
4. J. C. Iriarte Galarregui, A. Tellechea Pereda, J. L. Martínez De Falcón, I. Ederra, R. Gonzalo, and P. De Maagt, "Broadband radar cross-section reduction using AMC technology," IEEE Trans. Antenn. Propag. **61**(12), 6136–6143 (2013).
5. E. V. Jull, J. W. Heath, and G. R. Ebbeson, "Gratings that diffract all incident energy*," J. Opt. Soc. Am. **67**(4), 557 (1977).
6. E. Jull and G. Ebbeson, "The reduction of interference from large reflecting surfaces," IEEE Trans. Antenn. Propag. **25**(4), 565–570 (1977).
7. K. A. Jose and K. G. Nair, "Reflector-backed perfectly blazed strip gratings simulate corrugated reflector effects," Electron. Lett. **23**(2), 86 (1987).
8. T. Mathew, D. S. Stephen, K. A. Jose, C. K. Aanandan, P. Mohanan, and K. G. Nair, "The performance of a novel simulated corrugated surface for the reduction of radar cross section," Microw. Opt. Technol. Lett. **6**(10), 615–617 (1993).
9. D. S. Stephen, T. Mathew, K. A. Jose, C. K. Aanandan, P. Mohanan, and K. G. Nair, "New Simulated Corrugated Scattering Surface Giving Wide-Band Characteristics," Electron. Lett. **29**(4), 329–331 (1993).
10. R. Marqués, F. Martín, and M. Sorolla, *Metamaterials with Negative Parameters: Theory, Design and Microwave Applications* (John Wiley & Sons, 2008).
11. M. Beruete, M. Navarro-Cía, M. Sorolla, and I. Campillo, "Planoconcave lens by negative refraction of stacked subwavelength hole arrays," Opt. Express **16**(13), 9677–9683 (2008).
12. B. Orazbayev, M. Beruete, and I. Khromova, "Tunable beam steering enabled by graphene metamaterials," Opt. Express **24**(8), 8848–8861 (2016).
13. D. Schurig, J. J. Mock, B. J. Justice, S. A. Cummer, J. B. Pendry, A. F. Starr, and D. R. Smith, "Metamaterial electromagnetic cloak at microwave frequencies," Science **314**(5801), 977–980 (2006).
14. A. Alù and N. Engheta, "Achieving transparency with plasmonic and metamaterial coatings," Phys. Rev. E Stat. Nonlin. Soft Matter Phys. **72**(1), 016623 (2005).
15. N. Yu, P. Genevet, M. A. Kats, F. Aieta, J. P. Tetienne, F. Capasso, and Z. Gaburro, "Light propagation with phase discontinuities: generalized laws of reflection and refraction," Science **334**(6054), 333–337 (2011).
16. L. Zhang, S. Mei, K. Huang, and C. W. Qiu, "Advances in full control of electromagnetic waves with metasurfaces," Adv. Opt. Mater. **4**(6), 818–833 (2016).
17. N. M. Estakhri and A. Alù, "Recent progress in gradient metasurfaces," J. Opt. Soc. Am. B **33**(2), 21–30 (2016).
18. P. Genevet, F. Aieta, M. Kats, R. Blanchard, G. Aoust, J.-P. Tetienne, Z. Gaburro, and F. Capasso, "Flat Optics:

#298247 https://doi.org/10.1364/OE.25.022905
Journal © 2017 Received 15 Jun 2017; revised 4 Aug 2017; accepted 7 Aug 2017; published 11 Sep 2017

Optics EXPRESS

Controlling Wavefronts With Optical Antenna Metasurfaces," IEEE J. Sel. Top. Quantum Electron. **19**(3), 4700423 (2013).
19. B. Orazbayev, N. Mohammadi Estakhri, A. Alù, and M. Beruete, "Experimental Demonstration of Metasurface-Based Ultrathin Carpet Cloaks for Millimeter Waves," Adv. Opt. Mater. **5**(1), 1600606 (2017).
20. Y. Zhang, L. Liang, J. Yang, Y. Feng, B. Zhu, J. Zhao, T. Jiang, B. Jin, and W. Liu, "Broadband diffuse terahertz wave scattering by flexible metasurface with randomized phase distribution," Sci. Rep. **6**(1), 26875 (2016).
21. D. C. Skigin, A. N. Fantino, and S. I. Grosz, "Phase resonances in compound metallic gratings," J. Opt. A, Pure Appl. Opt. **5**(5), S129–S135 (2003).
22. D. C. Skigin and R. A. Depine, "Transmission Resonances of Metallic Compound Gratings with Subwavelength Slits," Phys. Rev. Lett. **95**(21), 217402 (2005).
23. M. Beruete, M. Navarro-Cía, D. C. Skigin, and M. Sorolla, "Millimeter-wave phase resonances in compound reflection gratings with subwavelength grooves," Opt. Express **18**(23), 23957–23964 (2010).
24. M. Navarro-Cía, D. C. Skigin, M. Beruete, and M. Sorolla, "Experimental demonstration of phase resonances in metallic compound gratings with subwavelength slits in the millimeter wave regime," Appl. Phys. Lett. **94**(9), 91107 (2009).
25. A. N. Fantino, S. I. Grosz, and D. C. Skigin, "Resonant effects in periodic gratings comprising a finite number of grooves in each period," Phys. Rev. E Stat. Nonlin. Soft Matter Phys. **64**(1 Pt 2), 016605 (2001).
26. C. Molero, R. Rodriguez-Berral, F. Mesa, and F. Medina, "Dynamical Equivalent Circuit for 1-D Periodic Compound Gratings," IEEE Trans. Microw. Theory Tech. **64**(4), 1195–1208 (2016).
27. R. Marqués, F. Mesa, L. Jelinek, and F. Medina, "Analytical theory of extraordinary transmission through metallic diffraction screens perforated by small holes," Opt. Express **17**(7), 5571–5579 (2009).
28. F. Medina, F. Mesa, and R. Marques, "Extraordinary Transmission Through Arrays of Electrically Small Holes From a Circuit Theory Perspective," IEEE Trans. Microw. Theory Tech. **56**(12), 3108–3120 (2008).
29. S. I. Grosz, D. C. Skigin, and A. N. Fantino, "Resonant effects in compound diffraction gratings: Influence of the geometrical parameters of the surface," Phys. Rev. E - Stat. Nonlinear, Soft Matter Phys. **65**, 1–6 (2002).
30. M. Born, E. Wolf, and A. B. Bhatia, *Principles of Optics: Electromagnetic Theory of Propaqation Interference and Diffraction of Light* (Cambridge University, 1999).

1. Introduction

The ability to reduce the backscattering of an object is of high importance in a wide range of applications, such as radar and telecommunication systems, military applications, etc. There are several strategies to achieve a reduction of scattered back radiation (monostatic scattering). Probably the most intuitive and widely used technique is to absorb the incident power by a layer of a radar absorbing material (RAM) [1]. RAM solutions at THz can be made broadband (FBW > 100% for –10 dB reduction) using resonant systems [2], or complex metamaterial absorbers (FBW ≈90% for –10 dB reduction) [3]. However, in high power systems this approach could lead to a huge amount of absorbed energy dissipated as heat in the system. In order to protect the system electronics, this heat needs to be handled leading usually to heavy and voluminous final systems [1]. Moreover, RAM based solutions are not rigid and susceptible to degradation in harsh environments. Another technique, which circumvents the heating problem and can have a rigid metallic profile, is based on diffraction gratings [1,4] where the reflected power is redirected eliminating both specular reflection [5–7] and backscattering [8]. At difference with RAM solutions, gratings absorb only a small amount of the incident energy and can be used in high power systems. However, they are usually narrowband (FBW ≈25% for –10 dB reduction), limiting their use [9].

Recent advances in the fields of photonic crystals and metamaterials have opened new fascinating possibilities to engineer the electromagnetic properties of artificial media, giving researchers an unprecedented control over the propagation of electromagnetic waves not achievable with natural materials [10]. This has resulted in numerous innovative applications, such as beam shaping devices (lenses, squeezers, …) [11], beam steering devices [12] and even invisibility cloaks [13]. The latter, where the cloaking effect is achieved by completely eliminating the scattering from an object (not only monostatic scattering) [14] is a splendid example of how metamaterials can control the propagation of electromagnetic waves. However, since the lattice constant of the metamaterial inclusions is deeply subwavelength, fabrication generally becomes challenging in practice. More recently, with the appearance of metasurfaces (a monolayer of photonic artificial atoms which introduces an abrupt interfacial

Optics EXPRESS

phase and allows a full control over the reflected electromagnetic wave [15]), more practical and compact solutions have become feasible [16,17] keeping the attractive functionalities of shaping light wavefronts [18] and allowing scattering mitigation [19,20] in a relatively wide bandwidth. However, despite their numerous advantages, metasurfaces based on artificial atoms are still complex to manufacture, preventing their use in practical backscattering reduction applications.

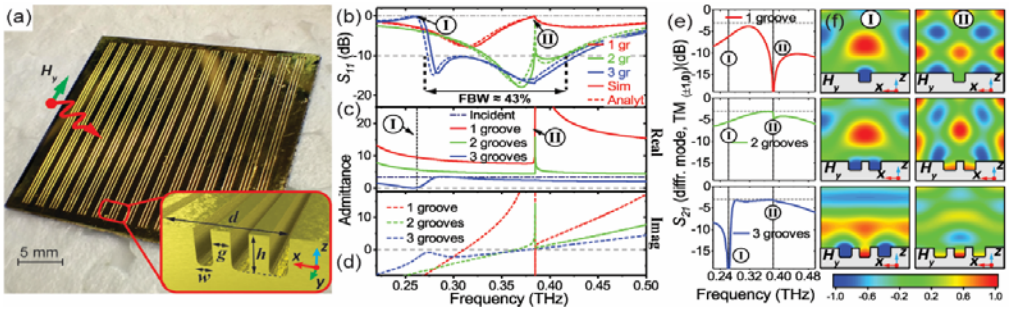

Fig. 1. (a) Fabricated prototype. Inset: unit cell geometry and parameters. (b) Comparison of analytical (dashed) and numerical (solid) reflection coefficient of a CRG with one (red), two (green) and three (blue) grooves. Analytical real (c) and imaginary (d) parts of the equivalent input admittance of the CRG with one (red), two (green) and three (blue) grooves. The admittance of the impinging wave is shown with dash-dotted dark blue line. (e) Simulation of the coupling from a normal incident plane wave to the first diffraction orders ($TM_{(\pm 1,0)}$) for a grating with one (red), two (green) and three (blue) grooves. The dashed gray line marks a level of –3 dB and is the maximum of the coupling to a diffraction order. (f) Snapshot of the magnetic field H_y at the highlighted frequencies: (I) f = 0.262 THz and (II) f = 0.384 THz.

Here we propose an alternative and less complex structure for backscattering reduction based on a metallic compound reflection grating (CRG), a structure that has been lately proposed, attracting the attention of the scientific community [21–25]. CRGs comprise a finite number of subwavelength grooves in each period. When the corrugations are deep enough cavity modes can be excited resulting in a strong field enhancement inside the grooves with different phases in adjacent grooves [21]. These phase resonances allow controlling the input impedance of the compound grating and, therefore, matching it to the wave impedance of free space [26] leading to a significant reduction of the backscattering, and giving rise to a transfer of energy to the grating lobes with maximized efficiency. Here, we experimentally demonstrate a wideband reduction of the backscattering using a CRG in THz range. Its performance is analyzed both in specular reflection and in the diffracted modes scattered by the structure. The measurements are compared with both analytical results, obtained using an equivalent circuit [26], and numerical results, demonstrating a reduction of the backscattering of –6 dB with a fractional bandwidth (FBW) of 57%.

2. Compound reflection grating design

The unit cell of the CRG (see inset of Fig. 1(a)) used in this work has a period d and consists of three grooves with the same depth h. The grooves have a width w and are separated by metallic walls with a thickness g and are carved in a gold wafer with conductivity $\sigma = 4.1 \times 10^7$ S/m. The structure is illuminated at normal incidence with a TM polarized (H_y parallel to the grooves) plane wave. As demonstrated in [26], this structure can be accurately described using an analytical equivalent circuit model [27,28] where each groove of the grating is represented as a short-circuited transmission line whose characteristic admittance depends on the groove width, w. This model allows obtaining the reflection coefficient as well as the diffracted modes with little computational effort and provides a straightforward explanation of the underlying physics. With this theoretical framework, it is easy to obtain the input admittance of the CRG as a function of the grooves parameters h, g, w, and d.

Optics EXPRESS

Using the equivalent circuit, a CRG with three grooves per period was optimized setting as target to have backscattering reduction in the broadest possible band, for a central frequency equal to f_0 = 0.35 THz (λ_0 = 857 μm) getting as a result the final dimensions shown in Table 1. In Fig. 1(b) is depicted the analytical reflection coefficient (S_{11}) magnitude of a CRG with one, two and three grooves (dashed red, green and blue lines respectively). The study was complemented with numerical results obtained using the frequency domain solver of the commercial software CST Microwave Studio® assuming unit cell boundary conditions, with a good agreement with the analytical results, see solid lines in Fig. 1(b).

From Fig. 1(b), it can be seen that the compound grating with three grooves is able to reduce the backscattering up to 10 dB within a FBW = 43%. The broadband performance of the CRG can be explained by the analytical model. The key point is to observe that the input admittance depends not only on the admittances of the grooves but also on the coupling between them. For several grooves (> 2) there are more degrees of freedom to tailor the input impedance enabling more control over the impedance [26]. As shown in Fig. 1(c), the input admittance of the CRG with three grooves has a real part (solid blue line) close to the admittance of the impinging wave, while the imaginary part (dashed blue line in Fig. 1(d)) is close to zero in a broad frequency range, leading to a good free space impedance matching and a low reflection level as corroborated in the blue lines of Fig. 1(b).

Table 1. Dimensions of the compound grating

Parameter	Designed, [μm]	Measured, [μm]
d	1560	1557
h	175	145*
g	135	128
w	207	215

* Estimated from the analytical calculation depth.

Note that contrarily to RAM-based solutions, the low reflection level is not due to absorption in the structure, as demonstrated by the small imaginary value of the admittance that accounts for low dissipation of the CRG. In the proposed structure, the power is transferred to diffracted high order modes. This is displayed in Fig. 1(e) (solid blue line). The mechanism is as follows: due to the symmetry imposed by the normal incidence, in the CRG with one or two identical grooves the fields inside must be equal in all grooves. This fact prevents the incident wave from exciting the grooves with different phases, which in terms of the equivalent circuit model means that the grooves have identical admittances. This limits the control of the equivalent input impedance of the CRG and therefore cannot provide a wideband impedance matching with free space (see Fig. 1(c)). This results in a low efficiency of the energy transfer to the diffracted modes (see solid red and green lines in Fig. 1(e)) and, therefore, in a higher level of backscattering. On the other hand, in a CRG with three (or more) cavities the grooves can be excited with different phases. Therefore, by properly tuning the grooves' dimensions one can achieve good impedance matching along with an efficient coupling to higher order diffraction modes reducing largely the specular reflection.

The analysis of the CRGs can be completed with the field analysis of Fig. 1(f) that shows the magnetic field (H_y) distribution. Two interesting points can be highlighted in Fig. 1(b-d): (I) f = 0.262 THz and (II) 0.384 THz. At (I) a peak of perfect specular reflection (dashed blue line in Fig. 1(b)) appears, which is attributed to a phase resonance (π resonance) of the CRG [21,25,29] since the fields in adjacent cavities have a phase difference of π, as clearly seen in Fig. 1(f) (third row, first column). From the analytical circuit model, we find this reflection peak coincides with a vanishing real part of the equivalent admittance (see Fig. 1(c)). In CRGs with one or two grooves the cavities are also excited, see Fig. 1(f). However, since they do not support a π resonance, the grooves simply diffract the incident wave with low efficiency (see red and green lines in Fig. 1(e)) with a high reflections level, due to the mismatched input admittance of the CRGs.

Optics EXPRESS

At the second point (II), a high reflectance peak related to the onset of the second diffraction order appears for one and two grooves. From the equivalent circuit model we find that both real and imaginary parts of the admittance tend to infinity (see Fig. 1(c-d)), i.e. the CRG behaves as a short-circuit. This is confirmed in the 1-groove field analysis of Fig. 1(f) (first row, second column). The incident wave does not excite the field inside the cavity and is totally reflected. On the other hand, with 3-grooves the fields excited inside the cavities have different amplitude and phase. Then, an efficient coupling of the incident wave to the diffraction modes is enabled (due to the impedance matching with free space). Furthermore, the analytical model also predicts a high level of reflection with 2-grooves due to the high value of the equivalent admittance. However, from the numerical results it can be seen that the field is excited inside the grooves and the reflection coefficient is low. We attribute this disagreement to the approximations made in the analytical equivalent circuit model, where we consider only the fundamental TEM mode inside the grooves with a uniform field distribution, since the grooves are subwavelength, and the field between and outside the grooves is neglected. This results in the clear high peak of the real and imaginary parts of the admittance (see Fig. 1(c,d)) and therefore in a low coupling to diffraction modes. However, from Fig. 1(e) it is obvious that the field inside the grooves is not uniform, and there is some coupling between grooves. This more complex field distribution leads to the disagreement between the models and for wider and closer grooves could cause a bigger discrepancy.

3. Experimental results

To prove experimentally the previous findings, a CRG was fabricated by photolithography followed by a deep reactive ion etching on a silicon substrate using a Plasma PRO NGP80 system. Afterwards, the obtained sample was sputtered with a thin layer of Au (250 nm, $\sigma = 4.1 \times 10^7$ S/m). At the lowest frequency limit (f_{min} = 0.22 THz) the skin depth is around t_{skin} = 170 nm, so this structure can be considered fully metallic. The parameters of the fabricated sample (except the depth h of the grooves) were measured using a microscope, showing some deviations from the optimal design (see Table 1) worsening the performance of the CRG, as shown next. The prototype has 15 periods and total dimensions 30 mm × 30 mm.

The spectrum of S_{11} parameter for a normally incident wave with TM polarization (H_y) was measured in the frequency range 0.22–0.5 THz, using external millimeter-wave heads of OML™ connected to an Agilent Technologies N5242A PNA-X network analyzer. A sketch of the used setup is shown in Fig. 2(a). High gain horn antennas were used to illuminate the fabricated CRG and obtain the S_{11} parameter, covering the whole frequency range. The transmitting horn antenna was placed a distance L_1 = 400 mm away from the sample to ensure uniform illumination. The experimentally measured S_{11} is shown in Fig. 2(b) (solid red line).

From this figure, it is obvious that the backscattering is reduced over a broad frequency band. The specular reflection is below –6 dB for almost the whole bandwidth, 0.3–0.5 THz. However, the level of backscattering reduction is worse compared to the optimal design (< –10 dB, see dotted gray line), due to the deviations in the manufacturing process. From the analytical model it can be shown that the performance of the CRG is more sensitive to the height of the grooves (not measured with the microscope) than the rest of parameters [26,29]. To verify this, the experimental results were compared with analytical and simulation results for different values of h, using the fabricated dimensions w, g, d and keeping the rest of parameters (σ, polarization, incidence angle, boundary conditions) as in the previous calculations. Since the analytical model allows to quickly solve the problem (in a matter of few seconds), it is possible to find the parameter h that gives better agreement with the experimental results. We found that a value h = 145 μm fitted the measured spectrum as shown in Fig. 2(b). The agreement between analytical, numerical and experimental curves is very good, confirming our previous statement about the fabrication errors in the grooves' height. Moreover, in all the curves a peak of almost perfect reflection related to the π

Optics EXPRESS

resonance in the grooves, is present (see Fig. 2(b)). From these results a FBW ≈57% can be estimated for S_{11} < –6 dB.

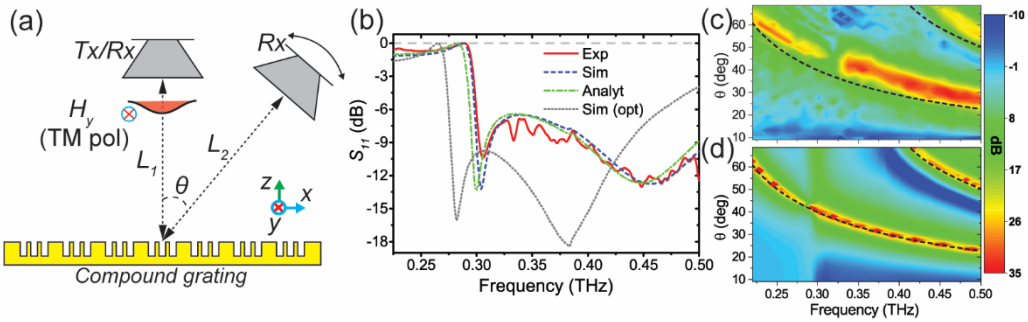

Fig. 2. (a) Schematic view of the experimental setups. (b) Reflection coefficient spectra for experimental (solid red line), numerical (dashed red line) and analytical (dotted blue line) results. The analytical and numerical results are obtained for d = 1557 µm, g = 128 µm, w = 215 µm and the groove height h = 145 µm. The reflection coefficient for the optimal parameters (d = 1560 µm, g = 135 µm, w = 207 µm and h = 175 µm) is shown with dotted gray line. Normalized radiation patterns: (c) experimental and (d) simulation results; the black dashed lines are the analytical positions of the grating lobes of order (m = 1) and (m = 2).

Next, in order to demonstrate the transfer of the reflected power to the grating lobes, the radiation patterns of the scattered field in the angular span of 9 – 69° were measured using the setup shown in Fig. 2(a). The experimental radiation patterns are shown in Fig. 2(c), with a good qualitative agreement with the simulation results (see Fig. 2(d)). Quantitatively, the small displacement of the grating lobes from the theoretical angles (see dashed lines in Fig. 2(c), which represent the analytical solutions for the grating lobes) can be explained by small misalignments in the setup (between the sample and the transmitter) that lead to oblique incidence (instead of normal) on the grating. From Fig. 2(c) we estimate an incidence angle α ≈4° using the grating equation [30]. This small deviation in α does not affect much the reflection coefficient, a fact that has been confirmed numerically (not shown here).

4. Conclusions

To sum up, in this work a CRG for backscattering reduction was designed, fabricated and measured. The experimental results were compared against analytical and numerical results, showing an excellent agreement between them. A wideband backscattering reduction of –6 dB was confirmed with FBW = 57%. The presented metallic CRG has a low-profile, relatively simple for practical realization design and provides an efficient transfer of the energy to diffracted modes. This makes it appealing for high-power systems, such as radar and telecommunication systems, with clear advantages over the conventional solutions based on RAM (which cause heating and therefore are voluminous and heavy) and conventional metallic gratings (which have narrow bandwidth).

Funding

MINECO (Project TEC2014-51902-C2-2-R); P.R.-U. sponsored by UPNA FPI PhD grant.

Acknowledgments

Thanks to Gonzalo Crespo and Juan Carlos Iriarte for help in fabrication and measurement.